Extreme Temperature Modeling of AlGaN/GaN HEMTs

Sayed Ali Albahrani, Dhawal Mahajan, *Student Member, IEEE*, Saleh Kargarrazi, *Member, IEEE*, Dirk Schwantuschke, Thomas Gneiting, *Member, IEEE*, Debbie G. Senesky, *Senior Member, IEEE*, and Sourabh Khandelwal, *Senior Member, IEEE*

***Abstract*— The industry standard advanced SPICE model (ASM)-GaN compact model has been enhanced to model the GaN high electron mobility transistors (HEMTs) at extreme temperature conditions. In particular, the temperature dependence of the trapping behavior has been considered and a simplifying approximation in the temperature modeling of the saturation voltage in the ASM-GaN model has been relaxed. The enhanced model has been validated by comparing the simulation results of the model with the dc *I–V* measurement results of a GaN HEMT measured with chuck temperatures ranging from 22 °C to 500 °C. A detailed description of the modeling approach is presented. The new formulation of the ASM-GaN compact model can be used to simulate the circuits designed for extreme temperature environments.**

***Index Terms*— Compact models, gallium nitride, high electron mobility transistors (HEMTs), high-temperature modeling, physics-based models, semiconductor device measurement, semiconductor device modeling.**

I. Introduction

GaN-BASED HEMT devices have demonstrated outstanding performance across a wide range of RF and power applications during recent times. The literature [1]–[3] shows increasingly aggressive scaling of GaN devices, which has resulted in very promising high-speed devices with gate lengths as small as 20 nm and $f_T/f_{\max}$ exceeding 400 GHz [4]. Furthermore, the GaN power devices that can reliably operate with the drain–source voltage (V_{DS}) values of 600–650 V are widely available where they set the current benchmark for commercial GaN power devices. Current research [5]–[7] indicates that the focus for GaN power devices is aimed toward increasing device reliability, while achieving V_{DS} values in the kilovolt (kV) range.

While these technology trends bode well for the future of the GaN-based technology, there are certain device modeling challenges that arise with such advancements. One such challenge relates to the extreme-temperature modeling of these devices. Such extreme temperatures exceeding a value of 500 °C can be easily reached in certain niche applications such as automotives, turbine engines, and Venus and Mercury interplanetary missions [8]–[10].

High-temperature operation of the GaN high electron mobility transistors (HEMTs) up to 500 °C has been attempted in [11]–[16] using both Si and Sapphire as the substrates. At the same time, there have been reports of analytical modeling of the high-temperature operation of these HEMTs using hydrodynamic equations [17], Monte Carlo simulations of electron transport in GaN [18], and charge control analysis [19].

However, to maximize the utility of GaN transistors in the RF and power circuits, their accurate and speedy simulation is needed. Both these metrics of circuit simulation, i.e., the accuracy and the speed, are determined by the compact model describing the device. Many empirical models have been proposed for the GaN HEMTs, but they are not physics-based in nature [20], [21]. Physics-based models [22]–[24] have the intrinsic advantage of having few parameters. These parameters are directly or indirectly linked to the physical effects governing the device dynamics. Hence, their extraction in a physics-based model is relatively easier than that in the other models. The advanced SPICE model (ASM)-GaN physics-based compact model [22], [23] has recently been selected by the compact-model-coalition standardization process as an industry standard model for the GaN devices. The model showcases as a promising tool for improving the accuracy and versatility of today's power GaN-based circuit simulations. In addition to the core modeling of the dc-IV and intrinsic capacitances, in the ASM-GaN compact model, flicker noise, thermal noise, gate current in AlGaN/GaN HEMTs [25]–[27], trapping [23], and a capacitance model in the presence of different combinations of gate and source field plates [28], [29] are also modeled.

Measurement results of the characteristics of a GaN HEMT device fabricated at Stanford's XLab across a wide temperature range from 22 °C to 500 °C [16] show the need for modifying the temperature-scaling equations of the parameters

Manuscript received November 25, 2019; accepted December 13, 2019. Date of publication January 13, 2020; date of current version January 27, 2020. This work was supported by the German Federal Ministry of Education and Research in the Framework of the Project GaNScan under Grant 16ES0745. The review of this article was arranged by Editor G. Verzellesi. *(Sayed Ali Albahrani and Dhawal Mahajan contributed equally to this work.) (Corresponding authors: Sayed Ali Albahrani; Dhawal Mahajan.)*

Sayed Ali Albahrani and Dirk Schwantuschke are with the Fraunhofer Institute for Applied Solid State Physics (IAF), 79108 Freiburg, Germany (e-mail: albahrani.sayed@gmail.com).

Dhawal Mahajan and Sourabh Khandelwal are with the Department of Engineering, Macquarie University, Sydney, NSW 2109, Australia (e-mail: dhawal.mahajan@students.mq.edu.au).

Saleh Kargarrazi and Debbie G. Senesky are with the Department of Aeronautics and Astronautics, Stanford University, Stanford, CA 94305 USA.

Thomas Gneiting is with AdMOS GmbH, 72636 Frickenhausen, Germany.

Color versions of one or more of the figures in this article are available online at http://ieeexplore.ieee.org.

Digital Object Identifier 10.1109/TED.2019.2960573

This work is licensed under a Creative Commons Attribution 4.0 License. For more information, see https://creativecommons.org/licenses/by/4.0/

of the ASM-GaN compact model to model the GaN HEMTs operating at extreme temperatures. In this work, we enhance the ASM-GaN compact model to capture the observed variations in the characteristics of the device with temperature. This article is organized as follows. Section II describes the structure of the device under test and presents the measurement results of the transfer characteristics of this device at various temperatures. Section III describes the modeling of the temperature dependences of the parameters of the ASM-GaN model and presents the excellent fit of the enhanced model to the measurement results. Section IV presents the simulation results of the enhanced ASM-GaN model and discusses several aspects of the modeling approach presented in this work. Finally, Section V draws the conclusions.

II. HEMT Structure and Measurement Results

The various geometries associated with the normally ON (i.e., depletion type) AlGaN-GaN HEMT device fabricated at the Stanford's XLab on Si substrate, used in this study, are as follows.

1) AlGaN-barrier thickness, $T_{\mathrm{BAR}} = 30$ nm.
2) Gate length, $L = 3\ \mu$m.
3) Gate width, $W = 20\ \mu$m.
4) Length of the gate–source access region, $L_{\mathrm{SG}} = 7\ \mu$m.
5) Length of the gate–source access region, $L_{\mathrm{DG}} = 7\ \mu$m.
6) Number of gate fingers, NF = 1.

We measured the dc drain-to-source current (I_{DS})–gate-to-source voltage (V_{GS}; transfer) characteristics of the above device at a wide range of ambient temperatures (T), ranging from $T = 22\ ^\circ$C to 500 °C. The results are shown in Figs. 1–5. Figs. 1–3 show the measured transfer transconductance-V_{GS} characteristics of three different drain-to-source voltages (V_{GS}). Each figure shows the measured characteristics at various temperatures. Fig. 4 shows the transfer characteristics at ambient temperatures $T = 22$ °C, 300 °C, and 500 °C, for drain-to-source voltages ranging from $V_{\mathrm{DS}} = 0.5$ to 5 V. In addition, Fig. 5 shows the I_{DS}–V_{DS} (output) characteristics at ambient temperatures $T = 22$ °C, 300 °C, and 500 °C, for the gate-to-source voltages ranging from $V_{\mathrm{GS}} = -4$ to 0 V, and the drain-to-source voltages ranging from $V_{\mathrm{DS}} = 0$ to 10 V

III. High-Temperature Device Modeling Using the ASM-GaN Compact Model

The ASM-GaN compact model in its current version incorporates temperature-scaling equations for several model parameters, namely, the channel's threshold voltage (VOFF), the carriers mobility (U0), and saturation velocity (VSAT) in the intrinsic and the drain and source access regions of the HEMT, the drain and source access regions' carrier densities (NS0ACSS), and the drain–source contact resistances (RC). The temperature-scaling equations for these model parameters are as follows:

$$\mathrm{VOFF}_t = \mathrm{VOFF}\ (1 - \mathrm{K_{T1}}\Delta\overline{T}) \quad (1)$$

$$\mathrm{U0}_t = \mathrm{U0}\ \overline{T}^{\mathrm{UTE}} \quad (2)$$

$$\mathrm{VSAT}_t = \mathrm{VSAT}\ \overline{T}^{\mathrm{AT}} \quad (3)$$

$$\mathrm{NS0ACC}_t = \mathrm{NS0ACC}(1 + \mathrm{K_{NS0}}\Delta\overline{T}) \quad (4)$$

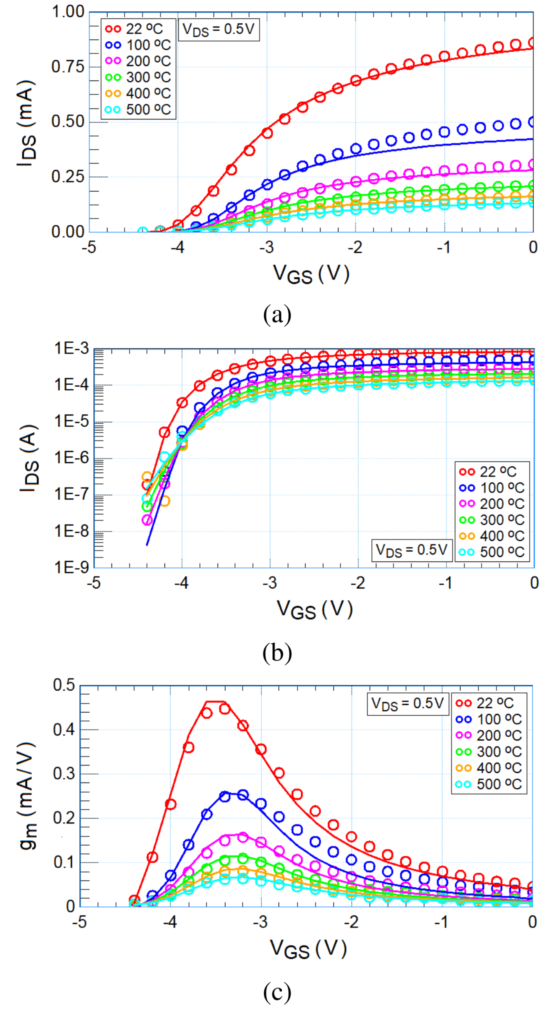

Fig. 1. Measured (symbol) and simulated (line) (a) I_{DS}–V_{GS} characteristics in linear scale, (b) I_{DS}–V_{GS} characteristics in semilogarithmic scale, and (c) g_m–V_{GS} characteristics, for temperatures ranging from 22 °C to 500 °C, with V_{GS} varying from −4.4 to 0 V and $V_{\mathrm{DS}} = 0.5$ V.

$$\mathrm{RC}_t = \mathrm{RC}(1 + \mathrm{K_{RC}}\Delta\overline{T}) \quad (5)$$

where

$$\overline{T} = T_{\mathrm{dev}}/T_{\mathrm{nom}} \quad (6)$$

$$\Delta\overline{T} = T_{\mathrm{dev}}/T_{\mathrm{nom}} - 1 \quad (7)$$

where T_{dev} [K] is the device temperature, which is the ambient temperature T plus the temperature due to self-heating, T_{nom} [K] is the nominal temperature, VOFF, U0, VSAT, NS0ACC, and RC are the model parameters at $T = T_{\mathrm{nom}}$, and $\mathrm{K_{T1}}$, UTE, AT, $\mathrm{K_{NS0}}$, and $\mathrm{K_{RC}}$ are the temperature parameters.

A schematic of the model used to describe the device under test, showing the temperature-dependent parameters associated with the different regions of the device, is shown in Fig. 6. As can be noted, the source and drain access regions are modeled in an identical manner, setting the 2-DEG density in both regions, denoted as NS0ACCS and NS0ACCD, equal to NS0ACC. Moreover, the electron mobility and saturation velocity of the source and drain access regions are set equal to those of the intrinsic region: U0ACCS = U0ACCD = U0 and VSATACCS = VSATACCD = VSAT. Furthermore,

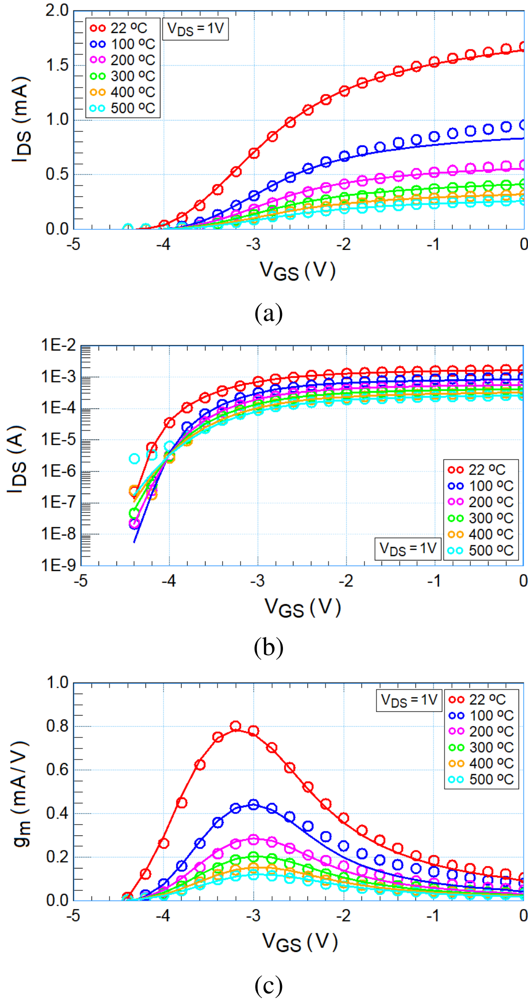

Fig. 2. Measured (symbol) and simulated (line) (a) I_{DS}–V_{GS} characteristics in linear scale, (b) I_{DS}–V_{GS} characteristics in semilogarithmic scale, and (c) g_m–V_{GS} characteristics, for temperatures ranging from 22 °C to 500 °C, with V_{GS} varying from −4.4 to 0 V and V_{DS} = 1 V.

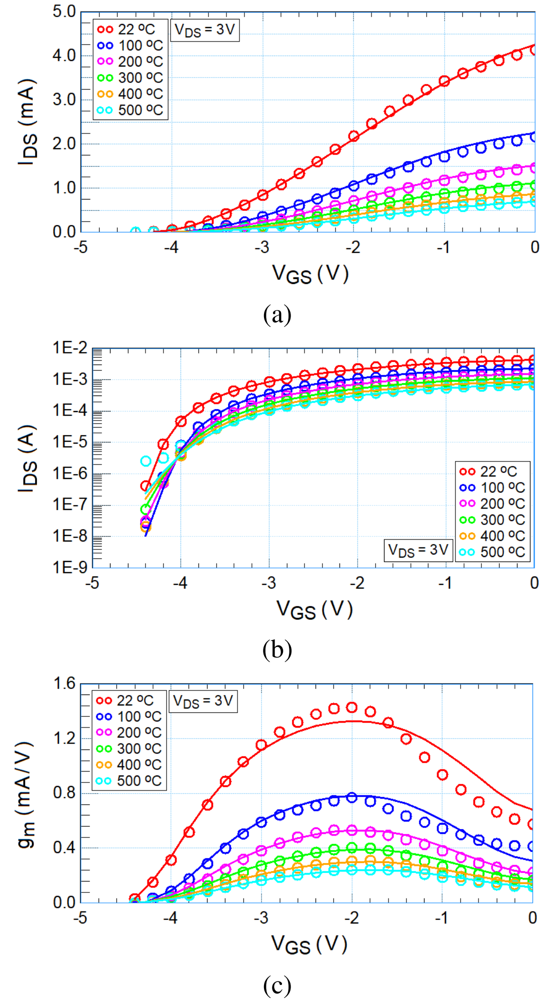

Fig. 3. Measured (symbol) and simulated (line) (a) I_{DS}–V_{GS} characteristics in linear scale, (b) I_{DS}–V_{GS} characteristics in semilogarithmic scale, and (c) g_m–V_{GS} characteristics, for temperatures ranging from 22 °C to 500 °C, with V_{GS} varying from −4.4 to 0 V and V_{DS} = 3 V.

the temperature parameters associated with NS0ACCS and NS0ACCD, denoted as $\mathrm{K_{NS0S}}$ and $\mathrm{K_{NS0D}}$, are set equal to $\mathrm{K_{NS0}}$, and the temperature parameters associated with the electron mobility and saturation velocity of the source and drain access regions are set equal to those of the intrinsic region: UTES = UTED = UTE and ATS = ATD = AT. Similarly, the source and drain access resistances are set equal to each other: RSC = RDC = RC, and the temperature parameters associated with these two parameters are also set equal to each other: $\mathrm{K_{RSC}} = \mathrm{K_{RDC}} = \mathrm{K_{RC}}$. All these different parameters have been introduced in the ASM-GaN model to capture the possible nonidealities within the device.

Another aspect of temperature modeling in the current version of the ASM-GaN model is as follows. High lateral electric field in the channel results in the saturation of the velocity of the electrons in the channel. Velocity saturation is modeled by modifying the expression for mobility as [30]

$$\mu_{\mathrm{eff}} = \beta_{\parallel}(\beta_{\perp}\mathrm{U0}_t) \tag{8}$$

where μ_{eff} is an effective mobility, $\mathrm{U0}_t$ is the low-field mobility and is given by (2), $\beta_{\perp}$ is the mobility-degradation coefficient due to the vertical electric field in the channel, neglecting the lateral electric field in the channel, and $\beta_{\parallel}$ is the mobility-degradation coefficient due to the lateral electric field in the channel and is given by

$$\beta_{\parallel} = \frac{1}{\sqrt{1+\left(\frac{\beta_{\perp}\mathrm{U0}_t}{\mathrm{VSAT}_t}E_{\parallel}\right)^2}} \tag{9}$$

where VSAT_t, given by (3), is the saturation velocity and $E_{\parallel}$ is the lateral electric field, which can be taken as

$$E_{\parallel} = (\psi_d - \psi_s)/L \tag{10}$$

where ψ_d and ψ_d are the surface potentials at the drain end and source end of the channel, respectively, and L is the gate length. Using (8), (10) can be written as

$$\mu_{\mathrm{eff}} = \frac{\beta_{\perp}\mathrm{U0}_t}{\sqrt{1+[(\psi_d-\psi_s)/V_{D\mathrm{sat}}]^2}} \tag{11}$$

where

$$V_{D\mathrm{sat}} = \frac{\mathrm{VSAT}_t L}{\beta_{\perp}\mathrm{U0}_t}. \tag{12}$$

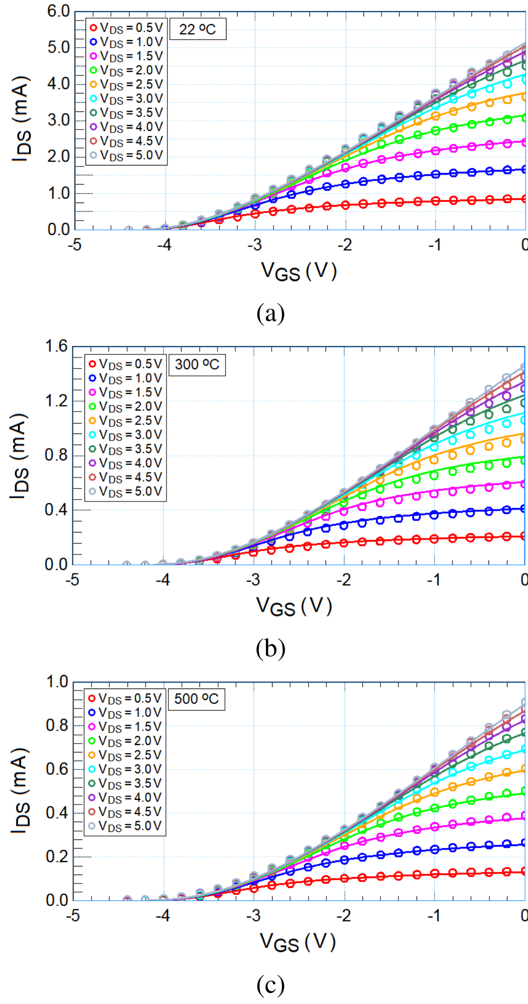

Fig. 4. Measured (symbol) and simulated (line) I_{DS}–V_{GS} characteristics in linear scale, at ambient temperature (a) $T = 22$ °C, (b) $T = 300$ °C, and (c) $T = 500$ °C, at drain-to-source voltages V_{DS} varying from 0.5 to 5 V.

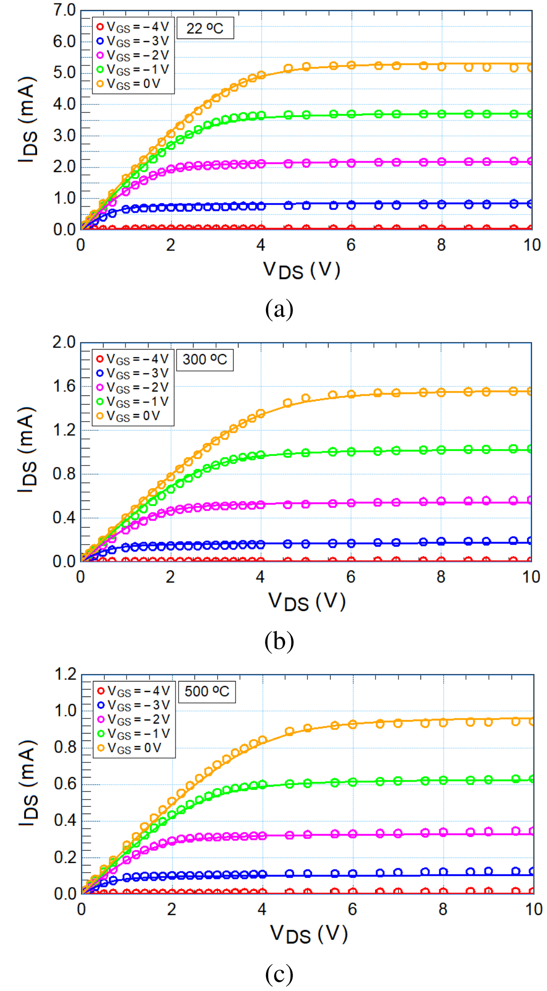

Fig. 5. Measured (symbol) and simulated (line) I_{DS}–V_{DS} characteristics in linear scale, at ambient temperature (a) $T = 22$ °C, (b) $T = 300$ °C, and (c) $T = 500$ °C, at gate-to-source voltages V_{GS} varying from −4 to 0 V.

The term $V_{D\text{sat}}$, which clearly is temperature-dependent, is also used in the ASM-GaN model to calculate an effective drain–source potential

$$V_{D\text{eff}} = \frac{V_{\text{DS}}}{\sqrt{1 + (V_{\text{DS}}/V_{D\text{sat}})^2}} \tag{13}$$

which is used in the place of the drain–source potential V_{DS} in the calculation of ψ_d. The above expression for μ_{eff} has been approximated in the ASM-GaN model as

$$\mu_{\text{eff}} = \frac{\beta_{\perp}\text{U0}_t}{\sqrt{1 + [\text{THESAT}(\psi_d - \psi_s)]^2}} \tag{14}$$

where THESAT, which is equal to $\beta_{\perp}\text{U0}_t/(\text{VSAT}_t L)$, has been set as a model parameter. As can be noted, this approximation amounts to neglecting the temperature dependence of THESAT. To accurately model the extreme-temperature conditions, we implemented (11) in the enhanced version of the ASM-GaN model, which we are presenting in this work.

In order to investigate the behavior of the device under test with temperature, we set the temperature parameters K_{T1}, UTE, AT, and K_{NS0} to zero and the parameters RC and K_{RC} to their measured values of 0.68 $\Omega \cdot$ mm and 0.45,

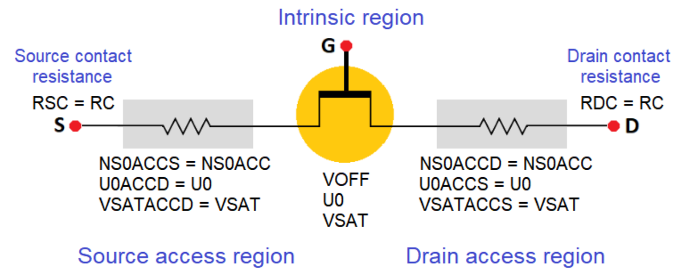

Fig. 6. Schematic of the model used to describe the device under test, showing the temperature-dependent parameters associated with the different regions of the device.

and extracted the parameters of the model at each temperature, using the same values for all the model parameters, except for the four parameters: VOFF, U0, VSAT, and NS0ACC. To avoid the influence of self-heating, we extracted these parameters at relatively low values of V_{DS}, in particular, at $V_{\text{DS}} = 0.5$–5 V. The variations of these parameters are shown in Fig. 7. Equations (2) and (3) fit well to the variations of the extracted values of U0 and VSAT, respectively, with UTE$= -1.975$ and AT$= 0$. It remains, therefore, to modify the temperature-scaling equations of VOFF and NS0ACC.

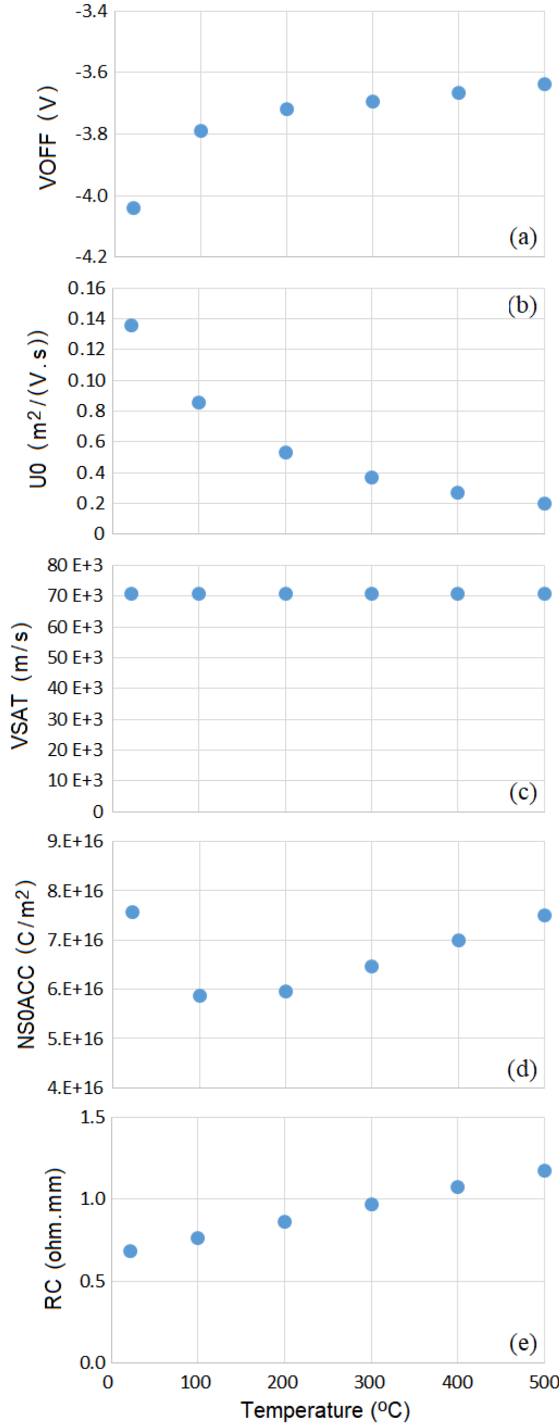

Fig. 7. Extracted values of (a) VOFF, (b) U0, (c) VSAT, (d) NS0ACC, and (e) RC for the device under test at $T = 22$ °C, 100 °C, 200 °C, 300 °C, 400 °C, and 500 °C.

The nonlinear variations of VOFF and NS0ACC with temperature, which for NS0ACC is nonmonotonic, can be modeled considering the presence of a trap center in the device under test, which is subject to injection of electrons, resulting in the ionization of this trap center and, hence, variation in the 2-DEG density in the channels of the intrinsic and access regions of the device under test.

Following the approach, we presented in [23] for the modeling of the trapping effect, the steady-state potential $\overline{v}_x$ introduced by traps acting as an electron-trapping center is given by [23]

TABLE I
EXTRACTED PARAMETERS OF THE ASM-GaN MODEL

	Description	Value
RTH0	Thermal Resistance (K/W)	25
EPSILON	Dielectric permittivity of AlGaN layer (F/m)	106.6e-12
VOFF	Cut-off voltage (V)	-4.04
NFACTOR	Sub-voff slope parameter	0.85
ETA0	DIBL Parameter	35.8e-3
VDSCALE	DIBL Scaling V_{DS}	2
U0	Low field mobility (m^2/(V . s))	135.5e-3
UA	Mobility degradation coefficient-first order	0
UB	Mobility degradation coefficient-second order	0
VSAT	Saturation velocity (m/s)	70.7e3
NS0ACC	2-DEG charge density in the source/drain access region (C/m)	7.8e16
RC	Source/drain contact resistance (ohm . m)	0.68e-3

TABLE II
TEMPERATURE PARAMETERS

	Description	Value
UTE	Temperature dependence of mobility	-1.975
AT	Temperature Dependence for saturation velocity	0
K_{RC}	Temperature dependence of source (drain) contact resistance	0.45
K_{T1}	Temperature dependence for VOFF	22e-3
K_{NS0}	Temperature dependence for 2-DEG charge density at source (drain) access region	300.6e-3

TABLE III
TRAPPING-RELATED PARAMETERS

	Description	Value
ϕ	Potential barrier (eV)	0.99
α	Proportionality constant in the equaiton of injection current (A/K^2)	862.6e6
K_{T1X}	Constant relating trap potential to VOFF	-66.9e-3
K_{NS0X}	Constant relating trap potential to NS0ACC	-334.8e-3

$$\overline{v}_X = V_X/[1 + \exp(-\phi_n)] \tag{15}$$

where V_x is the trap potential when the traps are fully ionized and

$$\phi_n = \ln(\alpha \mid I_{\text{Inj}} \mid) \tag{16}$$

where α is a constant and I_{Inj} is the electron current injected toward the trap center. We have found that an excellent fit to the measurement results can be obtained with an injection current of the following form:

$$I_{\text{Inj}} = \alpha T_{\text{dev}}^2 \exp(-q\phi/V_{\text{th}}) \tag{17}$$

where $V_{\text{th}} = K_B\ T_{\text{dev}}$ is the thermal voltage, where K_B is Boltzmann's constant and T_{dev} is the device temperature, and α and the potential barrier ϕ are the model parameters. It is worth noting that thermionic-emission current, which is given by the equation below [31], reduces to the above equation under the bias conditions at which the device under test was measured

$$I_{\text{TE}} = NFWLJ_{\text{TE0}}[\exp(V/(\eta V_{\text{th}})) - 1] \tag{18}$$

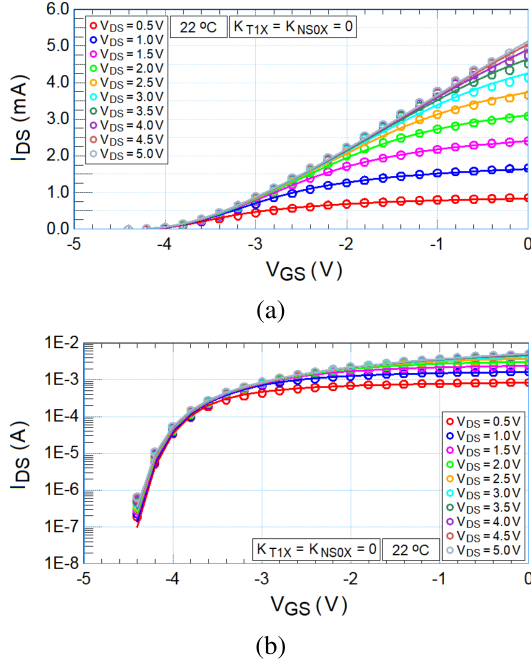

Fig. 8. Measured (symbol) and simulated (line) $I_{\rm DS}$–$V_{\rm GS}$ characteristics in (a) linear scale and (b) semilogarithmic scale, at ambient temperature $T = 22$ °C and at $V_{\rm DS}$ varying from 0.5 to 5 V, where the model is for when KT1X $= K$NS0X $= 0$.

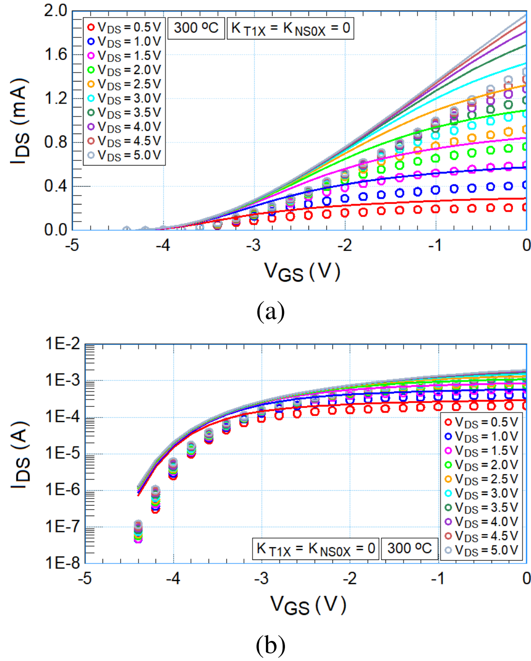

Fig. 9. Measured (symbol) and simulated (line) $I_{\rm DS}$–$V_{\rm GS}$ characteristics in (a) linear scale and (b) semilogarithmic scale, at ambient temperature $T = 300$ °C, at $V_{\rm DS}$ varying from 0.5 to 5 V, where the model is for when $\rm K_{T1X} = K_{NS0X} = 0$.

where NF is the number of fingers, η is the ideality factor, V is the applied voltage across the Schottky barrier, which can be set equal to the average of the intrinsic gate-to-source voltage ($V_{G_iS_i}$) and gate-to-drain voltage ($V_{G_iD_i}$), and $J_{\rm TE0}$ is the reverse saturation current density and is given by

$$J_{\rm TE0} = A^* T_{\rm dev}^2 \exp(-q\phi_{\rm TE}/V_{\rm th}) \tag{19}$$

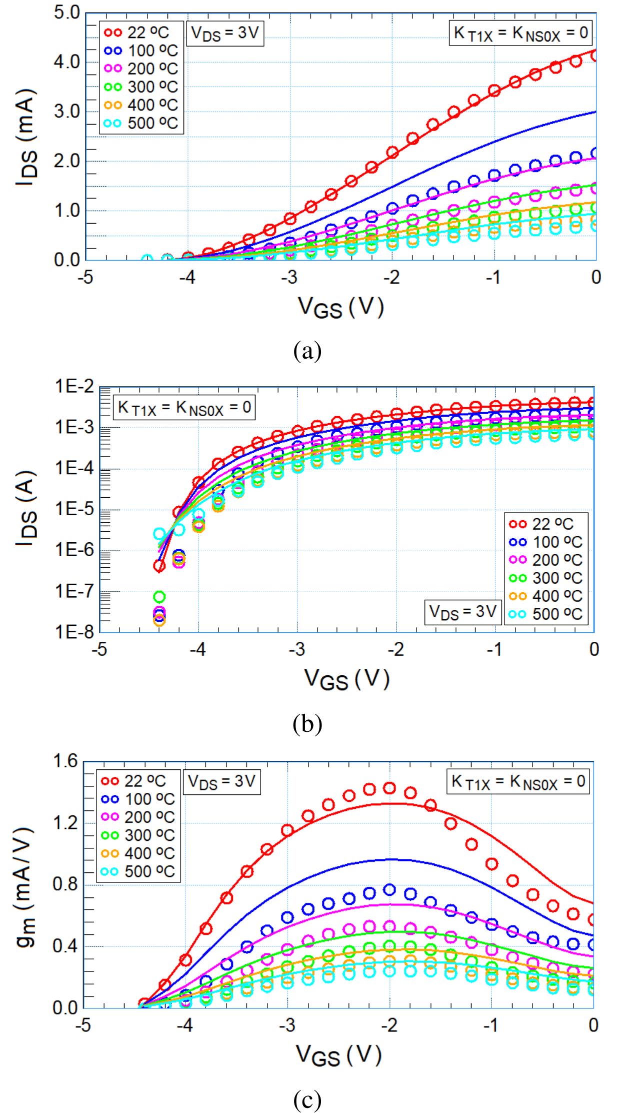

Fig. 10. Measured (symbol) and simulated (line) (a) $I_{\rm DS}$–$V_{\rm GS}$ characteristics in linear scale, (b) $I_{\rm DS}$–$V_{\rm GS}$ characteristics in semilogarithmic scale, (c) g_m–$V_{\rm GS}$ characteristics at $V_{\rm DS} = 3$ V, for temperatures ranging from 22 °C to 500 °C, where the model is for when $\rm K_{T1X} = K_{NS0X} = 0$.

where A^* is the effective Richardson's constant and $\phi_{\rm TE}$ is the Schottky barrier height. In particular, for $V_{G_iS_i}, V_{G_iD_i} < 0$

$$|\, I_{\rm TE}\, | \approx NFWL J_{\rm TE0}. \tag{20}$$

We then let the trap potential modify the parameters VOFF and NS0ACC of the ASM-GaN model in a linear manner as

$$\mathrm{VOFF}_x = \mathrm{VOFF}(1 + \mathrm{K_{T1X}}\bar{\bar{v}}_X) \tag{21}$$

$$\mathrm{NS0ACC}_x = \mathrm{NS0ACC}(1 + \mathrm{K_{NS0X}}\bar{\bar{v}}_X) \tag{22}$$

where $\bar{\bar{v}} = \bar{v}/V_x$ is the normalized steady-state trap potential to the potential V_x, and $\rm K_{T1X}$ and $\rm K_{NS0X}$ are the model parameters, implying that the first-order corrections to VOFF and NS0ACC are sufficient to capture the effect of trapping. The nonlinear variations of VOFF and NS0ACC with temperature, which for NS0ACC is nonmonotonic, are then modeled by modifying (1) and (4) as

$$\mathrm{VOFF}_t = \mathrm{VOFF}_x(1 - \mathrm{K_{T1}}\Delta\overline{T}) \tag{23}$$

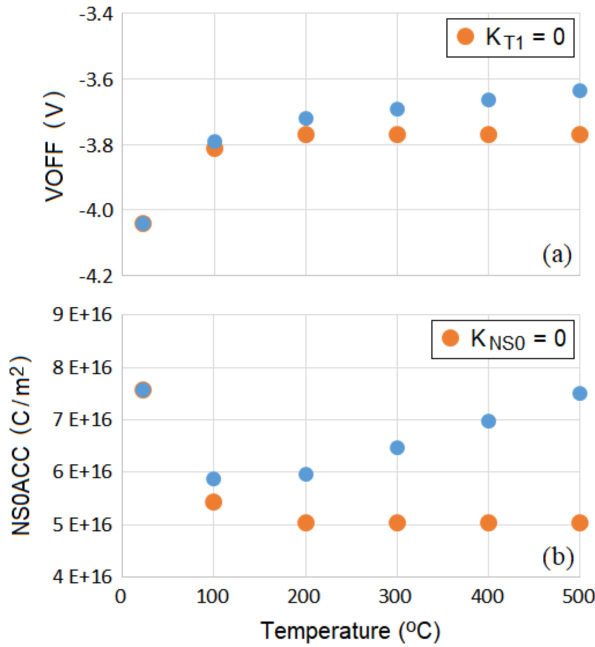

Fig. 11. Variations of the parameter (a) VOFF and (b) NS0ACC of the model with temperature, setting the temperature parameter (a) K_1 and (b) K_{NS0} to zero. The actual extracted variations of VOFF and NS0ACC are shown in blue.

$$\text{NS0ACC}_t = \text{NS0ACC}_x(1 + \text{K}_{\text{NS0}}\Delta\overline{T}). \tag{24}$$

IV. Results and Discussion

The results of the fit of the ASM-GaN compact model with the modified temperature-scaling equations to the measurement results are shown in Figs. 1–5. The different model parameters associated with this model are tabulated in Tables I–III.

In order to show the effect of temperature dependence of trapping, we simulated the model at $V_{DS} = 0$ V and at $T = 22$ °C and 300 °C, at the drain-to-source voltages ranging from $V_{DS} = 0.5$ to 5 V, with the trapping parameters K_{T1X} and K_{NS0X} set to zero. The results are shown in Figs. 8 and 9. Note from Fig. 8 that, at $T = 22$ °C, at which thermionic-emission current, which possibly is the injection current leading to charge trapping in the device under test, is very low, a good fit of the model to the measurement results is still obtained after setting K_{T1X} and K_{NS0X} to zero. Furthermore, we simulated the model at $V_{DS} = 3$ V, at ambient temperatures ranging from $T = 22$ °C to 500 °C, with the trapping parameters K_{T1X} and K_{NS0X} set to zero. The results are shown in Fig. 10.

In order to show the variations of VOFF_x and NS0ACC_x, given by (21) and (22), with temperature, we simulated the model with the temperature parameters K_{T1} and K_{NS0} set to zero. The results are shown in Fig. 11.

The nonlinear behavior depicted in Fig. 7(a) and (d) (and also in Fig. 11), which in Fig. 7(d) is nonmonotonic, is modeled with the application of the trapping model presented in [23], assuming the presence of a trap center with a given energy level. While we can model the data quite well with the model shown in [23], it is to be noted that the trapping model used here does not account for the trapping time constant, which requires performing measurements such as pulsed measurements, nor it accounts for multiple traps and their time constants. Nevertheless, we were able to model the dc behavior of the device under test over a wide range of temperatures with this simple trapping model. For the purposes of the studies performed for the device under test, (23) and (24) may also be viewed as the empirical extensions of the temperature equations used in the current version of the ASM-GaN model for the two parameters VOFF and NS0ACC.

V. Conclusion

Extreme temperature modeling of the measured dc transfer characteristics of a GaN HEMT was performed by enhancing the temperature-modeling aspect of the industry-standard ASM-GaN compact model. This was achieved by considering the temperature dependence of the trapping behavior of the device under test as well as relaxing an approximation invoked in the current version of the ASM-GaN model. A detailed description of the modeling approach and the excellent fit of the simulation results of the enhanced ASM-GaN model to the measurement results were presented. This model, which is capable of modeling devices for a wide temperature range, from 22 °C to 500 °C, can be effectively used in designing circuits and systems targeted at applications ranging from space to automobiles.

References

[1] D. F. Brown, Y. Tang, D. Regan, J. Wong, and M. Micovic, "Self-aligned AlGaN/GaN FinFETs," *IEEE Electron Device Lett.*, vol. 38, no. 10, pp. 1445–1448, Oct. 2017, doi: 10.1109/LED.2017.2747843.

[2] J. S. Moon, R. Grabar, M. Antcliffe, H. Fung, Y. Tang, and H. Tai, "High-speed FP GaN HEMT with f_T/f_{MAX} of 95/200 GHz," *Electron. Lett.*, vol. 54, no. 10, pp. 657–659, 2018, doi: 10.1049/el.2018.0417.

[3] S. D. Burnham *et al.*, "Reliability characteristics and mechanisms of HRL's T3 GaN technology," *IEEE Trans. Semicond. Manuf.*, vol. 30, no. 4, pp. 480–485, Nov. 2017, doi: 10.1109/TSM.2017.2748921.

[4] K. Shinohara *et al.*, "Scaling of GaN HEMTs and Schottky diodes for submillimeter-wave MMIC applications," *IEEE Trans. Electron Devices*, vol. 60, no. 10, pp. 2982–2996, Oct. 2013, doi: 10.1109/TED.2013.2268160.

[5] Y. Zhang *et al.*, "1200 V GaN vertical fin power field-effect transistors," in *IEDM Tech. Dig.*, Dec. 2017, pp. 9.2.1–9.2.4, doi: 10.1109/IEDM.2017.8268357.

[6] Y. Zhang *et al.*, "Large-area 1.2-kV GaN vertical power FinFETs with a record switching figure of merit," *IEEE Electron Device Lett.*, vol. 40, no. 1, pp. 75–78, Jan. 2019, doi: 10.1109/LED.2018.2880306.

[7] H. Amano *et al.*, "The 2018 GaN power electronics roadmap," *J. Phys. D, Appl. Phys.*, vol. 51, no. 16, Mar. 2018, Art. no. 163001, doi: 10.1088/1361-6463/aaaf9d.

[8] P. G. Neudeck, R. S. Okojie, and L.-Y. Chen, "High-temperature electronics-a role for wide bandgap semiconductors?" *Proc. IEEE*, vol. 90, no. 6, pp. 1065–1076, Jun. 2002, doi: 10.1109/JPROC.2002.1021571.

[9] T. George, K. A. Son, R. A. Powers, L. Y. Del Castillo, and R. Okojie, "Harsh environment microtechnologies for NASA and terrestrial applications," in *Proc. IEEE SENSORS*, Oct./Nov. 2005, p. 6, doi: 10.1109/ICSENS.2005.1597934.

[10] C.-M. Zetterling *et al.*, "Bipolar integrated circuits in SiC for extreme environment operation," *Semicond. Sci. Technol.*, vol. 32, 2017, Art. no. 034002, doi: 10.1088/1361-6641/aa59a7.

[11] W. Tan, M. Uren, P. Fry, P. Houston, R. Balmer, and T. Martin, "High temperature performance of AlGaN/GaN HEMTs on Si substrates," *Solid-State Electron.*, vol. 50, no. 3, pp. 511–513, 2006, doi: 10.1016/j.sse.2006.02.008.

[12] R. Cuerdo *et al.*, "High temperature behaviour of GaN HEMT devices on Si(111) and sapphire substrates," *Phys. Status Solidi C*, vol. 5, no. 6, pp. 1971–1973, 2008, doi: 10.1002/pssc.200778555.

[13] M. Akita, S. Kishimoto, and T. Mizutani, "High-frequency measurements of AlGaN/GaN HEMTs at high temperatures," *IEEE Electron Device Lett.*, vol. 22, no. 8, pp. 376–377, Aug. 2001, doi: 10.1109/55.936348.

[14] S. Arulkumaran *et al.*, "Temperature dependent microwave performance of AlGaN/GaN high-electron-mobility transistors on high-resistivity silicon substrate," *Thin Solid Films*, vol. 515, no. 10, pp. 4517–4521, 2007.

[15] S. Nuttinck, B. Banerjee, S. Venkataraman, J. Laskar, and M. Harris, "High temperature performances of AlGaN/GaN power HFETs," in *IEEE MTT-S Int. Microw. Symp. Dig.*, vol. 1, Jun. 2003, pp. 221–223, doi: 10.1109/MWSYM.2003.1210920.

[16] S. Kargarrazi, A. S. Yalamarthy, P. F. Satterthwaite, S. W. Blankenberg, C. Chapin, and D. G. Senesky, "Stable operation of AlGaN/GaN HEMTs for 25 h at 400°C in air," *IEEE J. Electron Devices Soc.*, vol. 7, pp. 931–935, Aug. 2019, doi: 10.1109/JEDS.2019.2937008.

[17] S. Vitanov, V. Palankovski, S. Maroldt, and R. Quay, "High-temperature modeling of AlGaN/GaN HEMTs," *Solid-State Electron.*, vol. 54, no. 10, pp. 1105–1112, 2010.

[18] J. D. Albrecht, R. P. Wang, P. P. Ruden, M. Farahmand, and K. F. Brennan, "Electron transport characteristics of GaN for high temperature device modeling," *J. Appl. Phys.*, vol. 83, no. 9, pp. 4777–4781, 1998, doi: 10.1063/1.367269.

[19] M. Huque, S. Eliza, T. Rahman, H. Huq, and S. Islam, "Temperature dependent analytical model for current–voltage characteristics of AlGaN/GaN power HEMT," *Solid-State Electron.*, vol. 53, no. 3, pp. 341–348, 2009, doi: 10.1016/j.sse.2009.01.004.

[20] I. Angelov *et al.*, "Large-signal modelling and comparison of AlGaN/GaN HEMTs and SiC MESFETs," in *Proc. Asia–Pacific Microw. Conf.*, Dec. 2006, pp. 279–282, doi: 10.1109/APMC.2006.4429422.

[21] L. Dunleavy, C. Baylis, W. Curtice, and R. Connick, "Modeling GaN: Powerful but challenging," *IEEE Microw. Mag.*, vol. 11, no. 6, pp. 82–96, Oct. 2010, doi: 10.1109/MMM.2010.937735.

[22] S. Khandelwal *et al.*, "ASM GaN: Industry standard model for GaN RF and power devices—Part 1: DC, CV, and RF model," *IEEE Trans. Electron Devices*, vol. 66, no. 1, pp. 80–86, Jan. 2019, doi: 10.1109/TED.2018.2867874.

[23] S. A. Albahrani, D. Mahajan, J. Hodges, Y. S. Chauhan, and S. Khandelwal, "ASM GaN: Industry standard model for GaN RF and power devices—Part-II: Modeling of charge trapping," *IEEE Trans. Electron Devices*, vol. 66, no. 1, pp. 87–94, Jan. 2019, doi: 10.1109/TED.2018.2868261.

[24] U. Radhakrishna, P. Choi, and D. A. Antoniadis, "Facilitation of GaN-based RF-and HV-circuit designs using MVS-GaN HEMT compact model," *IEEE Trans. Electron Devices*, vol. 66, no. 1, pp. 95–105, Jan. 2019, doi: 10.1109/TED.2018.2848721.

[25] A. Dasgupta, S. Khandelwal, and Y. S. Chauhan, "Compact modeling of flicker noise in HEMTs," *IEEE J. Electron Devices Soc.*, vol. 2, no. 6, pp. 174–178, Nov. 2014, doi: 10.1109/JEDS.2014.2347991.

[26] A. Dasgupta, S. Khandelwal, and Y. S. Chauhan, "Surface potential based modeling of thermal noise for HEMT circuit simulation," *IEEE Microw. Wireless Compon. Lett.*, vol. 25, no. 6, pp. 376–378, Jun. 2015, doi: 10.1109/LMWC.2015.2422472.

[27] S. Ghosh, A. Dasgupta, S. Khandelwal, S. Agnihotri, and Y. S. Chauhan, "Surface-potential-based compact modeling of gate current in AlGaN/GaN HEMTs," *IEEE Trans. Electron Devices*, vol. 62, no. 2, pp. 443–448, Feb. 2015, doi: 10.1109/TED.2014.2360420.

[28] S. A. Ahsan, S. Ghosh, K. Sharma, A. Dasgupta, S. Khandelwal, and Y. S. Chauhan, "Capacitance modeling in dual field-plate power GaN HEMT for accurate switching behavior," *IEEE Trans. Electron Devices*, vol. 63, no. 2, pp. 565–572, Feb. 2016, doi: 10.1109/TED.2015.2504726.

[29] S. A. Ahsan, S. Ghosh, S. Khandelwal, and Y. S. Chauhan, "Analysis and modeling of cross-coupling and substrate capacitances in GaN HEMTs for power-electronic applications," *IEEE Trans. Electron Devices*, vol. 64, no. 3, pp. 816–823, Mar. 2017, doi: 10.1109/TED.2017.2654264.

[30] S. Khandelwal and T. A. Fjeldly, "A surface-potential-based compact model for study of non-linearities in AlGaAs/GaAs HEMTs," in *Proc. IEEE Compound Semiconductor Integr. Circuit Symp. (CSICS)*, Oct. 2012, pp. 1–4, doi: 10.1109/CSICS.2012.6340055.

[31] S. M. Sze, "MIS diode and charge-coupled devices," in *Physics of Semiconductor Devices*. New York, NY, USA: Wiley, 2001, pp. 402–407.